Chapter 3

Biologically Inspired CPG-Based Locomotion Control System of a Biped Robot Using Nonlinear Oscillators with Phase Resetting

This chapter deals with a design for a locomotion control system of a biped robot inspired by the physiological concept of a central pattern generator (CPG). It shows the usefulness of the control system by stability analysis using a simple biped robot model and by various experiments using actual biped robots.

3.1. Introduction

In the robotics field, interest in the study of robots with legs has increased. However, these robots still have difficulties in establishing adaptive locomotor behaviors in various situations. In contrast, humans and animals produce adaptive walking in diverse environments by cooperatively and skillfully manipulating their complicated and redundant musculoskeletal systems, where neuromechanical interaction is crucial. To create new control strategies for legged robots, it is natural to use ideas inspired from biological systems. For that purpose, elucidating the mechanisms for creating adaptive locomotor

---

Chapter written by Shinya AOI.

behaviors in biological systems and constructing design principles to produce the adaptability in robotic systems are crucial issues.

Physiological studies have shown that the CPG in the spinal cord greatly contributes to rhythmic limb movement, such as locomotion [GRI 75, ORL 99, SHI 76]. So far, based on the physiological concept of the CPG, locomotion control systems of legged robots have been developed to create adaptive walking of the robots in various environments [IJS 07, IJS 08, LIU 08, KIM 07, NAK 04, NAK 06, NOM 09, STE 10].

The CPG can produce oscillatory behaviors even without rhythmic input and proprioceptive feedback. However, it must use sensory feedback to produce effective locomotor behavior. For example, spinal cats produce locomotor behaviors on a treadmill and their gait changes depending on the belt speed [FOR 73, ORL 99]. This result suggests that the tactile sensory information between their feet and belt influences the locomotion phase and its rhythm generated by the CPG [DUY 00]. Physiological evidence has shown that the locomotion rhythm and its phase are modulated by producing phase shift and rhythm resetting based on sensory afferents and perturbations (phase resetting) [CON 87, DUY 77, GUE 95, LAF 05, SCH 98]. Moreover, the functional roles of phase resetting in the generation of adaptive walking have been investigated using neuromusculoskeletal models of biological systems [AOI 10, YAK 04, YAM 03a, YAM 03b].

In this study, we design a simple locomotion control system for a biped robot using nonlinear oscillators based on the physiological concept of the CPG and physiological evidence of phase resetting. This control system produces adaptive locomotion of a biped robot. This study shows the usefulness of this locomotion control system from stability analysis using a simple biped robot model and from various experiments using actual biped robots.

3.2. Locomotion control system using nonlinear oscillators

3.2.1. *CPG-based locomotion control system*

The organization of the CPG in biological systems remains largely unclear. However, recent physiological findings suggest that the CPG consists of hierarchical networks composed of a rhythm generator (RG) and pattern formation (PF) networks [BUR 01, LAF 05, RYB 06a, RYB 06b]. The RG network generates the basic rhythm and alters it by producing phase shifts and rhythm resetting in response to sensory afferents and perturbations. The PF

network shapes the rhythm into spatiotemporal patterns of motor commands. The CPG separately controls the locomotor rhythm and motor commands in the RG and PF networks, respectively.

In this study, we develop a locomotion control system based on the two-layer hierarchical network model composed of the RG and PF networks. For the RG model, we produce the rhythm information for locomotor behavior using nonlinear oscillators and regulate the rhythm information based on phase resetting in response to touch sensor signals. For the PF model, we generate motor torques based on the rhythm information from the RG model to produce the joint movements. The following sections explain this locomotion control system.

3.2.2. *Rhythm generator model using nonlinear oscillators*

We construct the RG model to create rhythm information for the locomotor behavior through interactions of the robot mechanical system, the oscillator control system, and the environment. For this purpose, we use nonlinear oscillators to produce the basic locomotor rhythm, which is modulated by the phase resetting mechanism based on touch sensor signals.

We use an oscillator for the whole body, for each limb, or for each joint depending on the research objective. When we use an oscillator for each limb, the oscillators can manipulate the interlimb coordination pattern. When we use an oscillator for each joint, the oscillators can control the intralimb (intersegmental) coordination pattern, as well as the interlimb coordination pattern. In this study, we use an oscillator for the whole body for a simple biped robot model in section 3.3 and use an oscillator for each limb for actual biped robots in section 3.4.

When we use $N(\geq 1)$ oscillators (oscillator $1, \ldots, N$), we define ϕ_i ($i = 1, \ldots, N$) as the phase of the oscillator i, and employ the following phase dynamics:

$$\dot{\phi}_i = \omega + g_{1i} + g_{2i}, \quad i = 1, \ldots, N \qquad [3.1]$$

where ω is the basic oscillator frequency that uses the same value for all the oscillators; g_{1i} ($i = 1, \ldots, N$) is a function related to the interlimb and intralimb coordination (see section 3.2.4) and g_{2i} ($i = 1, \ldots, N$) is a function related to the phase and rhythm modulation based on the phase resetting mechanism in response to touch sensor signals (see section 3.2.5).

3.2.3. *Pattern formation model to determine the global parameters of limb kinematics*

Physiological evidence has shown that spinocerebellar neurons receive sensory signals from proprioceptors and cutaneous receptors and encode the global information of the limb kinematics, such as the length and orientation of the limb axis that connects from the root to the tip of the limb [BOS 01, POP 02, POP 03]. In this study, we construct the PF model to determine the desired limb kinematics based on the length and orientation of the limb axis from the oscillator state in the RG model and to produce motor torques for establishing the desired kinematics.

3.2.4. *Phase regulation based on interlimb and intralimb coordination*

For establishing stable bipedal locomotion, interlimb coordination is crucial. For example, both legs generally move in antiphase to prevent toppling over, both arms also move in antiphase, and one arm and the contralateral leg move in phase. When we use the oscillator i for the limb i and design the desired limb kinematics by the oscillator state, the interlimb coordination pattern is represented by the phase difference among the oscillators. Therefore, the function g_{1i} in [3.1] is given by:

$$g_{1i} = -\sum_j K_{ij} \sin(\phi_i - \phi_j - \Delta_{ij}), \quad i = 1, \ldots, N \qquad [3.2]$$

where Δ_{ij} is the desired phase relation between the oscillators i and j and K_{ij} is a gain constant.

When we use an oscillator for each joint, the function g_{1i} can be used to regulate the intralimb coordination in a similar manner.

3.2.5. *Sensory regulation based on phase resetting*

We modulate the locomotion rhythm and its phase based on the phase resetting mechanism in response to touch sensor signals to produce adaptive locomotion through dynamic interactions between the robot mechanical system, the oscillator control system, and the environment. The function g_{2i} in [3.1] corresponds to this modulation. When we use the oscillator i for the limb i and the limb i lands on the ground, the phase ϕ_i of the oscillator i is reset to ϕ_0 at the landing. Therefore, the function g_{2i} is written by:

$$g_{2i} = (\phi_0 - \phi_i)\delta(t - t_i^{\text{land}}), \quad i = 1, \ldots, N \qquad [3.3]$$

where t_i^{land} is the time when the limb i lands on the ground and $\delta(\cdot)$ denotes Dirac's delta function.

3.3. Stability analysis using a simple biped robot model

In this section, we show how the locomotion control system contributes to increasing stability and robustness for locomotion using a compass model as a simple biped robot model [AOI 06b, AOI 07b].

3.3.1. *Compass model*

Figure 3.1 shows the compass model composed of a body and two legs that are connected at the hip. We assume that masses are concentrated at the hip and the tips of the legs. The body mass is M, the leg mass is m and the leg length is l. This model is constrained on the $x-y$ plane and walks to the x-direction. The tip of the stance leg is constrained on the ground and the stance leg can only rotate around the tip. This model has two degrees of freedom, θ_1 and θ_2. θ_1 is the angle of the stance leg relative to the perpendicular line to the ground and is not directly controlled. On the other hand, θ_2 is the angle of the swing leg relative to the stance leg and is directly controlled by the input torque u. Acceleration due to gravity is g.

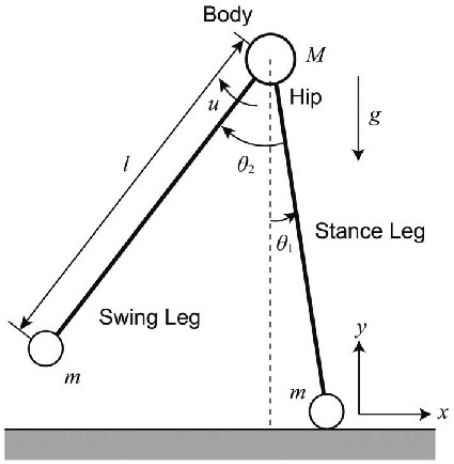

Figure 3.1. *Compass model*

The step cycle of the walking motion consists of two types of successive phases: swing and foot contact phases. In the following sections, we explain the governing equations for these phases.

3.3.1.1. *Swing phase model*

During the single-supported phase where the model is supported only by the stance leg and the swing leg is not in contact with the ground, the non-dimensional equation of motion is given by:

$$\begin{bmatrix} 1+2\beta(1-\cos\theta_2) & -\beta(1-\cos\theta_2) \\ -(1-\cos\theta_2) & 1 \end{bmatrix} \begin{bmatrix} \ddot{\theta}_1 \\ \ddot{\theta}_2 \end{bmatrix} + \begin{bmatrix} -\beta\sin\theta_2(\dot{\theta}_2^2 - 2\dot{\theta}_1\dot{\theta}_2) \\ -\dot{\theta}_1^2\sin\theta_2 \end{bmatrix} + \begin{bmatrix} \beta\sin(\theta_1-\theta_2) - \beta\sin\theta_1 - \sin\theta_1 \\ -\sin(\theta_1-\theta_2) \end{bmatrix} = \begin{bmatrix} 0 \\ u' \end{bmatrix} \quad [3.4]$$

where $\beta = m/M$, $\tau = \sqrt{g/l}t$, $u' = u/mgl$ and $\dot{x}$ indicates the derivative of x with respect to τ.

3.3.1.2. *Foot contact model*

When the leg touches the ground, the leg tip receives an impulsive force from the ground. For the foot contact model, we assume that the leg tip has no slip and no rebound at the foot contact and the double-supported phase duration is sufficiently short relative to the step cycle. That is, immediately following the foot contact, the tip of the swing leg is in turn constrained on the ground and the stance leg leaves the ground. In other words, the swing leg instantaneously becomes the stance leg, and vice versa, immediately after the foot contact.

The geometric condition the foot contact (Figure 3.2) is given by:

$$2\theta_1 - \theta_2 = 0 \quad [3.5]$$

Because the roles of the legs switch between the swing and stance legs just following the foot contact, the relationship of the angles between immediately before and after the foot contact is given by:

$$\begin{bmatrix} \theta_1^+ \\ \theta_2^+ \end{bmatrix} = \begin{bmatrix} -\theta_1^- \\ -\theta_2^- \end{bmatrix} \quad [3.6]$$

where $()^-$ indicates the state just before the foot contact and $()^+$ indicates the state just after the foot contact.

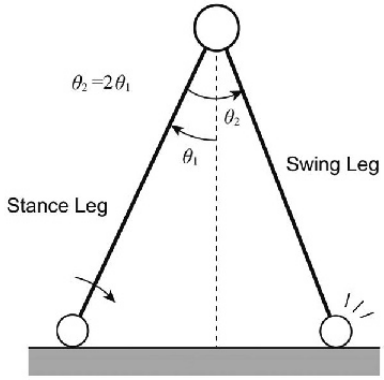

Figure 3.2. *Geometric condition for foot contact*

When the swing leg touches the ground, the leg tip receives an impact from the ground and the angular velocities suddenly change. We assume that the stance leg leaves the ground without interaction. From these assumptions, the angular velocities just after the foot contact are given by:

$$\begin{bmatrix} \dot{\theta}_1^+ \\ \dot{\theta}_2^+ \end{bmatrix} = \begin{bmatrix} \dfrac{2\cos 2\theta_1^-}{2+\beta(1-\cos 4\theta_1^-)}\dot{\theta}_1^- \\ \dfrac{2\cos 2\theta_1^-(1-\cos 2\theta_1^-)}{2+\beta(1-\cos 4\theta_1^-)}\dot{\theta}_1^- \end{bmatrix} \qquad [3.7]$$

3.3.2. *Locomotion control system*

We show how our locomotion control system is used for this compass model.

3.3.2.1. *Rhythm generator model*

Although the interlimb coordination plays important roles in achieving adaptive walking, we use only one oscillator for the RG model of the locomotion control system to keep the antiphase movements of the legs. Instead, we employ the amplitude of the oscillator, as well as the phase. We denote the amplitude and the phase of the oscillator by γ and ϕ, respectively. We use the following dynamics for the oscillator:

$$\begin{aligned} \dot{\gamma} &= 0 \\ \dot{\phi} &= \omega \end{aligned} \qquad [3.8]$$

Note that because we use only one oscillator, the function g_{1i} in [3.1] vanishes. The function g_{2i} in [3.1] is incorporated in section 3.3.2.3.

3.3.2.2. *Pattern formation model*

In the PF model of the locomotion control system, we construct the desired joint motion from the oscillator state and produce motor torque for establishing the desired joint motion. Because the compass model does not change the leg length, we design the desired joint motion based on the orientation of the limb axis and use a simple oscillation by:

$$\theta_{2\mathrm{d}} = \gamma \cos\phi + \gamma - s \qquad [3.9]$$

where s is a parameter that determines the stride angle. When we do not use phase resetting, we set $\gamma = s$.

To produce this desired joint angle, the input torque u' is given by:

$$u' = -\kappa(\theta_2 - \theta_{2\mathrm{d}}(\gamma, \phi)) - \sigma\dot{\theta}_2 \qquad [3.10]$$

where κ and σ are gain constants.

For the foot contact model, we switched the leg roles between swing and stance legs in [3.6]. We also need to switch the desired joint angle in [3.9] at the foot contact. When we do not use phase resetting, this is satisfied by the following conditions for the oscillator state:

$$\begin{bmatrix} \gamma^+ \\ \phi^+ \end{bmatrix} = \begin{bmatrix} \gamma^- \\ \phi^- - \pi \end{bmatrix} \qquad [3.11]$$

3.3.2.3. *Phase resetting model*

To incorporate the phase resetting mechanism, we reset the oscillator phase to ϕ_0 just after the foot contact. Instead of the function g_{2i} in [3.1], this is given by:

$$\phi^+ = \phi_0 \qquad [3.12]$$

Accompanied by this phase resetting, we modulate the oscillator amplitude to avoid inducing discrete change in the desired joint angle by:

$$\gamma^+ = \frac{2s - \gamma^-(1 + \cos\phi^-)}{1 + \cos\phi_0} \qquad [3.13]$$

Therefore, when we use phase resetting, we use [3.12] and [3.13] instead of [3.11].

3.3.3. *Periodic solution of the walking motion*

3.3.3.1. *Assumption for the controlled joint angle*

In this compass model, the joint angle θ_2 is controlled by a sufficient high-gain feedback control torque in [3.10]. We assume that the angle θ_2 is identical to the desired angle $\theta_{2\mathrm{d}}$ during locomotion, that is,

$$\theta_2 = \theta_{2\mathrm{d}}(\gamma, \phi) \qquad [3.14]$$

Under this assumption, we can denote the state variables as $q^{\mathrm{T}} = [\,\theta_1, \dot{\theta}_1, \gamma, \phi\,]$ and the equations of motion, the foot contact condition and the transition rule of the state variables from just before to just after a foot contact are summarized by:

$$\begin{cases} \dot{q} &= f(q), \quad q^- \notin S_{\mathrm{c}} \\ q^+ &= h(q^-), \quad q^- \in S_{\mathrm{c}} \end{cases} \qquad [3.15]$$

where $S_{\mathrm{c}} = \{\, q \,|\, r(q) = 2\theta_1 - \theta_{2\mathrm{d}}(\gamma, \phi) = 0 \,\}$ and

$$f(q) = \begin{bmatrix} f_1(q) \\ f_2(q) \\ f_3(q) \\ f_4(q) \end{bmatrix} = \begin{bmatrix} \dot{\theta}_1 \\ f_2(q) \\ 0 \\ \omega \end{bmatrix}$$

$$\begin{aligned} f_2(q) = {} & \{\beta(1-\cos\theta_{2\mathrm{d}})\ddot{\theta}_{2\mathrm{d}} + \beta\sin\theta_{2\mathrm{d}}(\dot{\theta}_{2\mathrm{d}}^2 - 2\dot{\theta}_1\dot{\theta}_{2\mathrm{d}}) \\ & -\beta\sin(\theta_1 - \theta_{2\mathrm{d}}) + \beta\sin\theta_1 + \sin\theta_1\}/\{1 + 2\beta(1-\cos\theta_{2\mathrm{d}})\} \end{aligned}$$

$$h(q) = \begin{bmatrix} h_1(q) \\ h_2(q) \\ h_3(q) \\ h_4(q) \end{bmatrix} = \begin{bmatrix} -\theta_1 \\ 2\cos 2\theta_1 \\ \dfrac{}{2 + \beta(1-\cos 4\theta_1)}\dot{\theta}_1 \\ h_3(q) \\ h_4(q) \end{bmatrix}$$

$$h_3(q) = \begin{cases} \gamma & \text{without resetting} \\ \dfrac{2s - \gamma(1+\cos\phi)}{1+\cos\phi_0} & \text{with resetting} \end{cases}$$

$$h_4(q) = \begin{cases} \phi - \pi & \text{without resetting} \\ \phi_0 & \text{with resetting} \end{cases}$$

3.3.3.2. *Approximate periodic solution using perturbation method*

Because the above equations can not be solved directly due to the strong nonlinearity, we attempt to solve them approximately and obtain the approximate periodic solution from just after a foot contact to just before the next foot contact. In particular, we consider the walking motion in which the tipping motion from the perpendicular line to the ground is small. In this case, the angles θ_1 and $\theta_{2\mathrm{d}}$ are small and hence we define $s = \varepsilon$ and $\gamma = \varepsilon\Gamma$ ($\Gamma = 1$ for the case without phase resetting), where ε is a small parameter. We use power-series expansions for the state variables θ_1 and ϕ by:

$$\begin{aligned} \theta_1(\tau) &= \varepsilon X_0(\tau) + \varepsilon^3 X_1(\tau) + \cdots \\ \phi(\tau) &= (\omega\tau + \Phi_0) + \varepsilon^2\Phi_1 + \cdots, \quad 0 \le \tau \le T \end{aligned} \qquad [3.16]$$

where T ($= O(1)$) is the step period, that is the time interval from just after a foot contact to just before the next foot contact, and $\tau = 0$ and T indicates the time just after a foot contact and just before the next foot contact, respectively. These expansions yield:

$$\theta_{2\mathrm{d}}(\gamma, \phi) = \varepsilon Y_0(\tau) + \varepsilon^3 Y_1(\tau) + \cdots, \quad 0 \le \tau \le T \qquad [3.17]$$

where

$$\begin{cases} Y_0(\tau) = \Gamma\cos(\omega\tau + \Phi_0) + \Gamma - 1 \\ Y_1(\tau) = -\Gamma\sin(\omega\tau + \Phi_0)\Phi_1 \\ \quad\vdots \end{cases}$$

By substituting [3.16] and [3.17] into the equation of motion in [3.15], we obtain:

$$\begin{aligned} &\varepsilon\big[\ddot{X}_0 - \beta Y_0 - X_0\big] + \varepsilon^3\Big[\ddot{X}_1 - \beta Y_1 - X_1 + \beta Y_0^2\ddot{X}_0 - \frac{\beta}{2}Y_0^2\ddot{Y}_0 + 2\beta\dot{X}_0\dot{Y}_0 Y_0 \\ &\quad -\beta\dot{Y}_0^2 Y_0 + \frac{\beta}{2}X_0^2 Y_0 - \frac{\beta}{2}X_0 Y_0^2 + \frac{\beta}{6}Y_0^3 + \frac{1}{6}X_0^3\Big] + O(\varepsilon^5) = 0 \end{aligned} \qquad [3.18]$$

where $X_i = X_i(\tau)$ and $Y_i = Y_i(\tau)$ ($i = 0, 1$). The substitution of the step period T and the state variables in [3.16] and [3.17] into the foot contact condition and transition rule in [3.15] gives the boundary condition and step

period for the approximate periodic solution by:

$$\begin{aligned}
&\varepsilon\Big[X_0(T)+\frac{1}{2}Y_0(0)\Big]+\varepsilon^3\Big[X_1(T)+\frac{1}{2}Y_1(0)\Big]+O(\varepsilon^5)=0\\
&\varepsilon\Big[X_0(0)-\frac{1}{2}Y_0(0)\Big]+\varepsilon^3\Big[X_1(0)-\frac{1}{2}Y_1(0)\Big]+O(\varepsilon^5)=0\\
&\varepsilon\big[\dot{X}_0(0)-\dot{X}_0(T)\big]+\varepsilon^3\big[\dot{X}_1(0)+4\beta X_0^2(T)\dot{X}_0(0)\\
&\qquad\qquad -\dot{X}_1(T)+2X_0^2(T)\dot{X}_0(T)\big]+O(\varepsilon^5)=0\\
&\varepsilon\big[Y_0(0)+Y_0(T)\big]+\varepsilon^3\big[Y_1(0)+Y_1(T)\big]+O(\varepsilon^5)=0\\
&T=\begin{cases}\dfrac{\pi}{\omega} & \text{without resetting}\\[2ex] \dfrac{\pi-2\phi_0}{\omega} & \text{with resetting}\end{cases}
\end{aligned} \qquad [3.19]$$

From [3.18] and [3.19], the equations for $X_0(\tau)$, Φ_0 and Γ are given by:

$$\begin{aligned}
&\ddot{X}_0(\tau)-\beta Y_0(\tau)-X_0(\tau)=0\\
&\begin{cases}X_0(T)=-\dfrac{1}{2}Y_0(0)\\ X_0(0)=\dfrac{1}{2}Y_0(0)\\ \dot{X}_0(0)=\dot{X}_0(T)\\ Y_0(0)=-Y_0(T)\end{cases}
\end{aligned} \qquad [3.20]$$

The solution is given by:

$$\begin{aligned}
X_0(\tau)&=\left(\frac{\beta}{\omega^2+1}+\frac{1}{2}\right)\left(\frac{e^{\tau}}{1-e^{T}}+\frac{e^{-\tau}}{1-e^{-T}}\right)\cos\Psi-\frac{\beta}{\omega^2+1}\cos(\omega\tau+\Psi)\\
Y_0(\tau)&=\cos(\omega\tau+\Psi)\\
\Psi&=\begin{cases}0 & \text{without resetting}\\ \phi_0 & \text{with resetting}\end{cases}
\end{aligned} \qquad [3.21]$$

($\Phi_0 = 0$ for the case without phase resetting, $\Phi_0 = \phi_0$ and $\Gamma = 1$ for the case with phase resetting). This solution corresponds to the solution when we linearize equation [3.15] with respect to the angles θ_1 and $\theta_{2\mathrm{d}}$. When $\phi_0 = 0$, the solutions without and with phase resetting become identical.

Next, from [3.18] and [3.19], the equations for $X_1(\tau)$ and Φ_1 are given by:

$$\ddot{X}_1 - \beta Y_1 - X_1 + \beta Y_0^2 \ddot{X}_0 - \frac{\beta}{2} Y_0^2 \ddot{Y}_0 + 2\beta \dot{X}_0 \dot{Y}_0 Y_0 - \beta \dot{Y}_0^2 Y_0 + \frac{\beta}{2} X_0^2 Y_0 - \frac{\beta}{2} X_0 Y_0^2 + \frac{\beta}{6} Y_0^3 + \frac{1}{6} X_0^3 = 0$$

$$\begin{cases} X_1(T) = -\dfrac{1}{2} Y_1(0) \\ X_1(0) = \dfrac{1}{2} Y_1(0) \\ \dot{X}_1(0) + 4\beta X_0^2(T) \dot{X}_0(0) = \dot{X}_1(T) - 2X_0^2(T) \dot{X}_0(T) \\ Y_1(0) = -Y_1(T) \end{cases} \quad [3.22]$$

The solution of Φ_1 becomes:

$$\Phi_1 = \begin{cases} \dfrac{e^T + 1}{e^T - 1} \dfrac{(1 + 2\beta)(1 + 2\beta + \omega^2)}{8\beta\omega} & \text{without resetting} \\ 0 & \text{with resetting} \end{cases} \quad [3.23]$$

The solution of $X_1(\tau)$ is so complicated that we do not display the details here. It concludes that the approximate periodic solution of the state variables θ_1 and ϕ and step period T becomes equivalent to:

$$\theta_1(\tau) = \varepsilon \left[\left(\frac{\beta}{\omega^2 + 1} + \frac{1}{2} \right) \left(\frac{e^\tau}{1 - e^T} + \frac{e^{-\tau}}{1 - e^{-T}} \right) \cos \Psi - \frac{\beta}{\omega^2 + 1} \cos(\omega\tau + \Psi) \right] + \cdots$$

$$\phi(\tau) = \begin{cases} \omega\tau + \varepsilon \dfrac{e^T + 1}{e^T - 1} \dfrac{(1 + 2\beta)(1 + 2\beta + \omega^2)}{8\beta\omega} + \cdots & \text{without resetting} \\ \omega\tau + \phi_0 & \text{with resetting} \end{cases}$$

$$T = \frac{\pi - 2\Psi}{\omega}$$

$$\Psi = \begin{cases} 0 & \text{without resetting} \\ \phi_0 & \text{with resetting} \end{cases} \quad [3.24]$$

Figures 3.3(a) and (b) show the periodic solution of this approximate analysis and computer simulation ($\beta = 0.2$, $\omega = 1.5$ rad and $\varepsilon = 6^\circ$) for without and with phase resetting, respectively. In the computer simulation, we do not assume that the controlled angle θ_2 is identical to the desired angle θ_{2d}

and we actually controlled the angle θ_2 by the high-gain feedback torque in [3.10]. These figures verify that the obtained approximate solution is close to the rigorous solution and that the approximate solution to $O(\varepsilon^3)$ is closer to the rigorous solution than that to $O(\varepsilon)$.

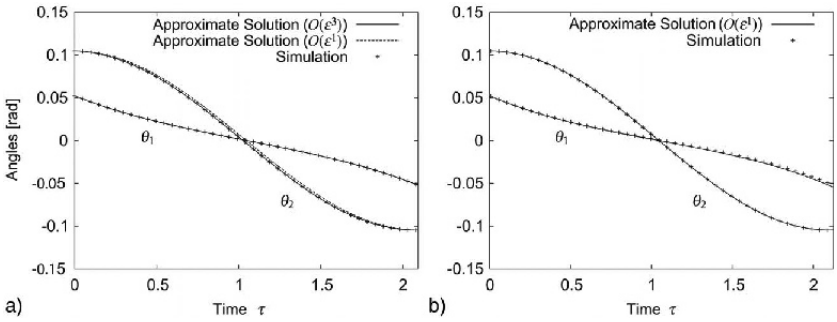

Figure 3.3. *Periodic solution of approximate analysis and computer simulation ($\beta = 0.2$, $\omega = 1.5$ rad and $\varepsilon = 6°$). a) Without phase resetting and b) with phase resetting ($\phi_0 = 0$)*

3.3.4. *Stability analysis*

Whether the obtained periodic solution is stable depends on the gait parameters, such as β and ω. We conduct a stability analysis using a Poincaré map to investigate it.

A Poincaré map is a return map from one point on the Poincaré section to the next point on the Poincaré section. Periodic behavior results in a fixed point on the Poincaré section and stability is determined from the eigenvalues of the Jacobian matrix of the Poincaré map around the fixed point. Periodic motion is asymptotically stable if all of the eigenvalues are inside the unit circle on the complex plane, that is, all of the magnitudes of the eigenvalues are less than 1.

3.3.4.1. *Jacobian matrix of the Poincaré map*

In our stability analysis, we use the state just after the foot contact as the state on the Poincaré section. In our compass model, the walking motion is governed by continuous and discrete equations. By considering such a hybrid structure, the Jacobian matrix of the Poincaré map is given by the product of three matrices, B, D and E, induced by the disturbances in the discrete changes due to the foot contact, the change in its timing and the evolved perturbations during the continuous equation [COL 97].

To obtain the Jacobian matrix of the Poincaré map, we first define the periodic solution as $q^*(\tau)$, the step period as τ^* and the perturbed state from the periodic solution $q^*(\tau)$ from just after a foot contact to just before the next foot contact as $q^*(\tau) + \delta q(\tau)$. Then, the matrices B and D are given by:

$$\begin{aligned} B &= \partial_q h(q^*(\tau^*)) \\ D &= I - \frac{\dot{q}^*(\tau^*)\partial_q r(q^*(\tau^*))^{\mathrm{T}}}{\partial_q r(q^*(\tau^*))^{\mathrm{T}}\dot{q}^*(\tau^*)} \end{aligned} \quad [3.25]$$

where $\partial_q = \partial/\partial q$ and I is an unit matrix. The substitution of the perturbed state $q^*(\tau) + \delta q(\tau)$ into the equation of motion [3.15] gives:

$$\delta\dot{q}(\tau) = \partial_q f(q^*(\tau))\delta q(\tau) \quad [3.26]$$

By integrating this equation from $\tau = 0$ to τ^*, the matrix E is derived from:

$$\delta q(\tau^*) = E\delta q(0) \quad [3.27]$$

The Jacobian matrix J of the Poincaré map is given by:

$$J = BDE \quad [3.28]$$

3.3.4.2. *Stability characteristics of the periodic solution without phase resetting*

When we do not use phase resetting, the amplitude of the oscillator remains constant ($\gamma = s$) during locomotion. Therefore, we use $q^{\mathrm{T}} = [\,\theta_1, \dot{\theta}_1, \phi\,]$ for the state variables to investigate stability of the periodic solution.

When we use the approximate solution in [3.24], the matrices B, D and E are given by the power series of parameter ε^2:

$$\begin{aligned} B &= B_0 + \varepsilon^2 B_1 + O(\varepsilon^4) \\ D &= D_0 + \varepsilon^2 D_1 + O(\varepsilon^4) \\ E &= E_0 + \varepsilon^2 E_1 + O(\varepsilon^4) \end{aligned} \quad [3.29]$$

This results in:

$$J = J_0 + \varepsilon^2 J_1 + O(\varepsilon^4) \quad [3.30]$$

where

$$J_0 = B_0 D_0 E_0$$
$$J_1 = B_1 D_0 E_0 + B_0 D_1 E_0 + B_0 D_0 E_1$$

The substitution of the approximate periodic solution gives:

$$J_0 = \begin{bmatrix} 0 & 0 & 0 \\ * & 1 - \beta\omega^2 d(\beta,\omega) & -\dfrac{\beta\omega}{1+\omega^2}\{2 - \beta\omega^2 d(\beta,\omega)\} \\ * & \omega(1+\omega^2) d(\beta,\omega) & 1 - \beta\omega^2 d(\beta,\omega) \end{bmatrix} \quad [3.31]$$

where

$$d(\beta,\omega) = \frac{e^{\pi/\omega} + e^{-\pi/\omega} - 2}{1 + 2\beta + \omega^2} > 0$$

and J_1 is so complicated that we do not display here.

First, we investigate the stability of the periodic solution based on the matrix J_0 obtained from the solutions $X_0(\tau)$ and Φ_0. That is, we employ only the first-order expansion of the state variables to approximately achieve the eigenvalues of the Jacobian matrix. The matrix J_0 has one zero eigenvalue ($\lambda_3 = 0$) and the other two eigenvalues $\lambda_{1,2}$ are given from the quadratic equation:

$$\lambda^2 - 2\{1 - \beta\omega^2 d(\beta,\omega)\}\lambda + 1 = 0 \quad [3.32]$$

Therefore, the eigenvalues $\lambda_{1,2}$ are given by:

$$\lambda_{1,2} = 1 - \beta\omega^2 d(\beta,\omega) \pm \sqrt{\{1 - \beta\omega^2 d(\beta,\omega)\}^2 - 1} \quad [3.33]$$

These eigenvalues are categorized according to the parameters β and ω as follows:

Case 1: $\lambda_{1,2}$ *are complex conjugate*

In this case, it follows that $0 < \beta\omega^2 d(\beta,\omega) < 2$ and the periodic solution is marginally stable from the following:

$$\lambda_1 \lambda_2 = \lambda\bar{\lambda} = |\lambda|^2 = 1 \quad [3.34]$$

Case 2: $\lambda_{1,2}$ *are real and distinct*

In this case, it follows that $\beta\omega^2 d(\beta,\omega) > 2$ and the periodic solution is unstable because there are stable and unstable eigenvalues from the following:

$$\begin{aligned}\lambda^2 - 1 &= 2\{1-\beta\omega^2 d(\beta,\omega)\}\lambda - 2 \\ &= 2\sqrt{\{1-\beta\omega^2 d(\beta,\omega)\}^2 - 1} \\ &\quad \times\left\{\sqrt{[1-\beta\omega^2 d(\beta,\omega)]^2-1} \pm [1-\beta\omega^2 d(\beta,\omega)]\right\} \gtrless 0\end{aligned} \qquad [3.35]$$

Case 3: $\lambda_{1,2}$ *are degenerate*

In this case, it follows that $\beta\omega^2 d(\beta,\omega) = 0, 2$ and the periodic solution is marginally stable from the following:

$$\lambda_{1,2} = 1, -1 \qquad [3.36]$$

This linear stability analysis concludes that the periodic solution is marginally stable for $\beta\omega^2 d(\beta,\omega) \leq 2$ and otherwise the periodic solution is unstable.

To investigate the relationship of the stability between the parameters β and ω, we define $g_0(\beta,\omega) = \beta\omega^2 d(\beta,\omega) - 2$. It follows that:

$$\begin{aligned}\frac{\partial g_0}{\partial \omega}(\beta,\omega) &= -\frac{\beta(1-e^{-\pi/\omega})}{(1+2\beta+\omega^2)^2}\Big[\pi(1+2\beta+\omega^2)(1+e^{\pi/\omega}) \\ &\qquad +2\omega(1+2\beta)(1-e^{\pi/\omega})\Big] < 0 \\ \frac{\partial g_0}{\partial \beta}(\beta,\omega) &= \omega^2(1+\omega^2)\frac{e^{\pi/\omega}+e^{-\pi/\omega}-2}{(1+2\beta+\omega^2)^2} > 0\end{aligned} \qquad [3.37]$$

In addition, it follows that:

$$\begin{aligned}\lim_{\omega\to+0} g_0(\beta,\omega) &= \infty \\ \lim_{\omega\to+\infty} g_0(\beta,\omega) &= -2 \\ \lim_{\beta\to+0} g_0(\beta,\omega) &= -2 \\ \lim_{\beta\to+\infty} g_0(\beta,\omega) &= \frac{1}{2}\left[\pi^2 - 4 + \sum_{n=2}^{\infty}\frac{2\omega^2}{(2n)!}\left(\frac{\pi}{\omega}\right)^{2n}\right] > 0\end{aligned} \qquad [3.38]$$

From [3.37], $g_0(\beta, \omega)$ is monotonically decreasing and increasing with respect to the parameters β and ω, respectively. Therefore, from [3.38], the parameter ω (>0) that satisfies $g_0(\beta, \omega) = 0$ exists and is unique for each parameter β (>0) and also the parameter β (>0) that satisfies $g_0(\beta, \omega) = 0$ exists and is unique for each parameter ω (>0). From the implicit function theorem, we can define functions $\omega = \omega_0(\beta)$ and $\beta = \omega_0^{-1}(\omega)$ such that $g_0(\beta, \omega_0(\beta)) = g_0(\omega_0^{-1}(\omega), \omega) = 0$. Thus, it concludes that the periodic solution is marginally stable for $\omega \geq \omega_0(\beta)$ or, equivalently, $\beta \leq \omega_0^{-1}(\omega)$. Figure 3.4 shows the function $\omega = \omega_0(\beta)$. This corresponds to the boundary between the marginally stable and unstable region for the parameters β and ω.

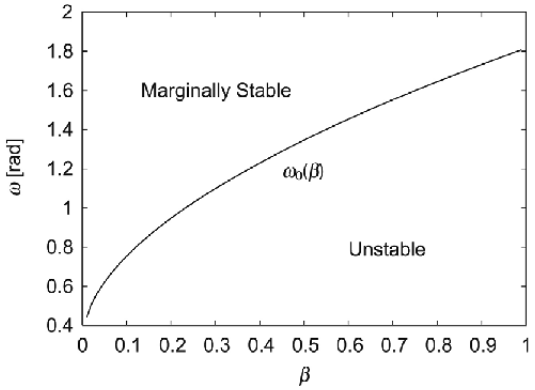

Figure 3.4. *Function $\omega = \omega_0(\beta)$. This is the boundary between the marginally stable and unstable regions with respect to the parameters β and ω*

This linear stability analysis reveals that the periodic solution is marginally stable or unstable depending on the parameters β and ω. The marginal stability result may be applicable in the limit when $\varepsilon = 0$ and the tipping motion and the stride of the walking motion disappear. However, marginal stability is a fragile feature and this analysis is inconclusive and insufficient to clarify the actual stability characteristics when $\varepsilon > 0$. Therefore, to examine the actual stability characteristics, we next achieve more rigorous eigenvalues of the Jacobian matrix by employing the second-order expansion of the state variables and matrix J_1.

Figure 3.5 shows the contour of the maximum magnitude among three eigenvalues $\lambda_{1,2,3}$ of the matrix J to $O(\varepsilon^2)$ with respect to the parameters β and ω for $\varepsilon = 6°$, where the thick line is the function $\omega = \omega_0(\beta)$. The maximum magnitude among the eigenvalues in the parameter region where we obtained the marginal stability in the first step of the stability analysis slightly decreases from 1, revealing that the periodic solution is asymptotically stable.

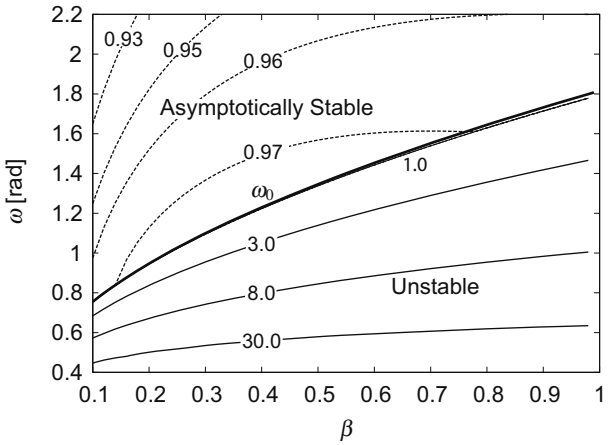

Figure 3.5. *Contour of the maximum eigenvalue magnitude when we consider the higher order of the power-series expansions for the matrix J ($\varepsilon = 6^\circ$). Thick line shows the function $\omega = \omega_0(\beta)$*

3.3.4.3. *Stability improvement due to phase resetting*

When we use phase resetting, the amplitude of the oscillator is modulated based on the foot contact event. Therefore, we use $q^{\mathrm{T}} = [\,\theta_1, \dot{\theta}_1, \gamma, \phi\,]$ for the state variables to investigate stability of the periodic solution.

The substitution of the approximate periodic solution reveals that the matrix J_0 has two zero eigenvalues ($\lambda_{3,4} = 0$) and the other two eigenvalues $\lambda_{1,2}$ are obtained from the equation:

$$\lambda^2 - 2a_1\lambda + a_2 = 0 \qquad [3.39]$$

where

$$a_1 = \frac{1}{2\dot{X}_0^- - \dot{Y}_0^-}\left\{ -\ddot{X}_0^- E_- + \dot{X}_0^-\left(E_+ - \frac{1-\cos\phi_0}{1+\cos\phi_0}\right) + \frac{\dot{Y}_0^-}{1+\cos\phi_0}\left[\frac{\beta}{\omega^2+1}((E_+ + 1)\cos\phi_0 - E_-\omega\sin\phi_0) + \beta(E_+ - 1)\right]\right\}$$

$$a_2 = \frac{1}{2\dot{X}_0^- - \dot{Y}_0^-}\left\{\dot{Y}_0^- + \frac{2\dot{Y}_0^-}{1+\cos\phi_0}\left[\frac{\beta}{\omega^2+1}((E_+ + 1)\cos\phi_0 - E_-\omega\sin\phi_0) - \beta(E_+ - 1)\right] - 2\frac{1-\cos\phi_0}{1+\cos\phi_0}(\dot{X}_0^- E_+ - \ddot{X}_0^- E_-)\right\}$$

$$E_+ = \frac{e^T + e^{-T}}{2},\ E_- = \frac{e^T - e^{-T}}{2}$$
$$\dot{X}_0^- = \dot{X}_0(T),\ \ddot{X}_0^- = \ddot{X}_0(T),\ \dot{Y}_0^- = \dot{Y}_0(T)$$

The eigenvalues $\lambda_{1,2}$ are obtained by the function of the parameters β, ω and ϕ_0 and given by:

$$\lambda_{1,2}(\omega, \beta, \phi_0) = a_1 \pm \sqrt{a_1^2 - a_2} \quad [3.40]$$

First, and in particular, we consider the case when $\phi_0 = 0$. In this case, [3.40] becomes equivalent to:

$$\lambda_{1,2}(\omega, \beta, 0) = 1 - \beta\omega^2 d(\beta, \omega),\ 0 \quad [3.41]$$

These eigenvalues reveal that the periodic solution is asymptotically stable for $\beta\omega^2 d(\beta, \omega) < 2$ and the periodic solution is unstable for $\beta\omega^2 d(\beta, \omega) > 2$. Regarding the stability region of the parameters β and ω, this result is the same as the case in which we do not use phase resetting. However, the stability is improved. Figures 3.6(a) and (b) show the maximum magnitude of the eigenvalues for the parameters β and ω in the cases without and with phase resetting, respectively, revealing that the stability is improved by employing phase resetting.

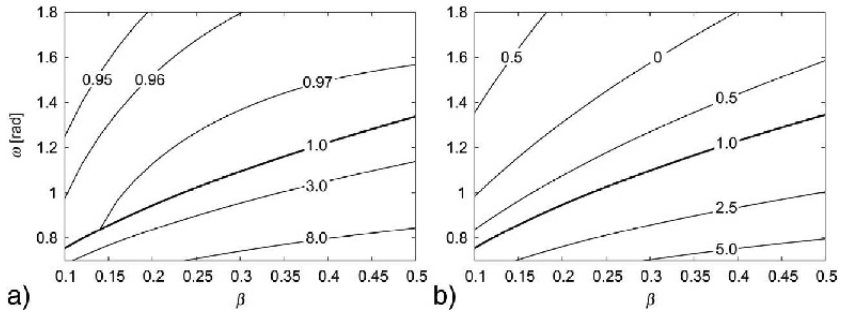

Figure 3.6. *Contour of the maximum eigenvalue magnitude with respect to the parameters β and ω. a) Without phase resetting and b) with phase resetting ($\phi_0 = 0$)*

Next, we consider the case that includes $\phi_0 \neq 0$. Figure 3.7 shows the transition of the stability region for the parameters β and ω due to the parameter ϕ_0, and the comparison of the analytic and the simulation results ($\varepsilon = 6°$).

This reveals that the asymptotic stability region is enlarged by increasing the parameter ϕ_0.

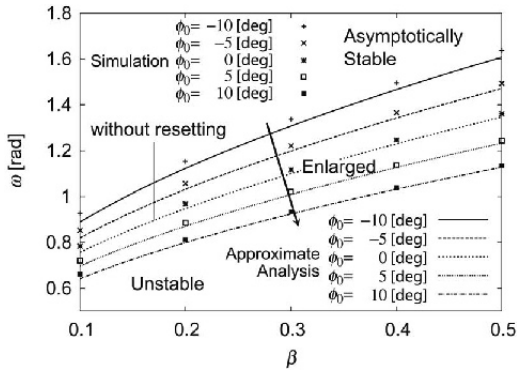

Figure 3.7. *Transition of the stability for the parameter* ϕ_0

When the parameter ϕ_0 exceeds a critical value, which depends on the parameters β and ω, the appearance of the stability region significantly changes. When the parameter ϕ_0 is less than the critical value, the decrease of β or/and the increase of ω increases the stability of the periodic motion and there is only one boundary with respect to the parameters β and ω, which divides into asymptotically stable and unstable regions as shown in Figure 3.7. On the other hand, when the parameter ϕ_0 is beyond the critical value, another boundary appears and the asymptotically stable region is formed between two unstable regions for the parameters β and ω, as shown in Figure 3.8. Therefore, in that case there is a region where the decrease of β or/and the increase of ω decreases the stability and thus it is necessary to use an adequate value for the parameter ϕ_0.

We focus on the stability to achieve such parameter ϕ_0. Figures 3.9(a) and (b) show the maximum magnitude of the eigenvalues versus the parameter ϕ_0 with respect to the parameters β and ω, respectively, revealing that it has an extreme value for the parameter ϕ_0. Therefore, we use it as an optimal value of the parameter ϕ_0. Such optimal value ϕ_0^* is obtained by the condition $a_1^2 - a_2 = 0$. Particularly when the optimal value ϕ_0^* is small, from the linear analysis it is given by:

$$\phi_0^* = \frac{(1-\beta\omega^2 d)^2}{\beta(1-\beta\omega^2 d)\left\{\dfrac{16}{1+2\beta+\omega^2} - (\omega^2-4)d\right\} - 2} \qquad [3.42]$$

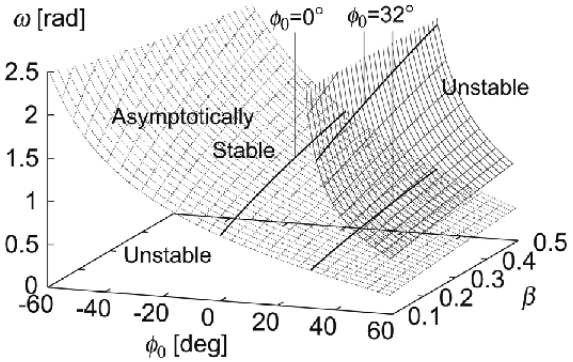

Figure 3.8. *Stability region for the parameters with phase resetting*

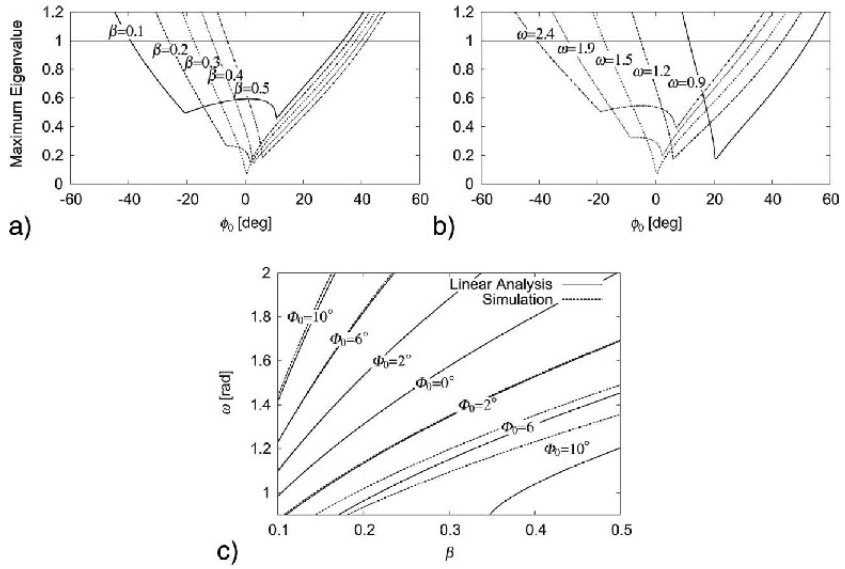

Figure 3.9. *Maximum magnitude of the eigenvalues for the parameter ϕ_0 a) for the parameter β ($\omega = 1.5$ rad) and b) for the parameter ω ($\beta = 0.2$)). c) Optimal value ϕ_0^* for the parameters β and ω*

Figure 3.9(c) shows the optimal value ϕ_0^* for the parameters β and ω obtained by the linear analysis and the rigorous computer simulation. This analysis concludes that resetting the phase of the oscillator into an adequate value and modifying the walking motion due to phase resetting based on the touch sensor signals increases the stability of the walking motion.

An analytical approach to show the improvement of stability and robustness of locomotion due to phase resetting is also conducted using a more plausible five-link biped robot model, which has torso and knee joints [AOI 11b]. In addition, the compass model used in this study shows period-doubling bifurcations leading to chaos by the parameters β and ω, similar to that observed in passive dynamic walking [GAR 98, GOS 98], where approximate analysis using perturbation method is useful to clarify stability characteristics inherent in locomotion dynamics [AOI 06a].

3.4. Experiment using biped robots

In this section, we show how the locomotion control system produces adaptive walking through the experiments using actual biped robots.

3.4.1. *Locomotion control system*

First, we show how our locomotion control system is used for actual biped robots.

3.4.1.1. *Rhythm generator model*

We denote the left and right legs by leg 1 and leg 2, respectively, and also denote the left and right arms by arm 1 and arm 2, respectively. For the RG model, we use six phase oscillators (leg 1, leg 2, arm 1, arm 2, trunk and inter oscillators). We define $\phi_{\rm L}^i$, $\phi_{\rm A}^i$, $\phi_{\rm T}$ and $\phi_{\rm I}$ ($i = 1, 2$) as the phases of the leg i, arm i, trunk and inter oscillators, respectively, and use the following dynamics for the phase dynamics [3.1]:

$$\begin{aligned}
\dot{\phi}_{\rm I} &= \omega + g_{1\rm I} \\
\dot{\phi}_{\rm T} &= \omega + g_{1\rm T} \\
\dot{\phi}_{\rm A}^i &= \omega + g_{1\rm A}^i + g_{2\rm A}^i \quad i = 1, 2 \\
\dot{\phi}_{\rm L}^i &= \omega + g_{1\rm L}^i + g_{2\rm L}^i \quad i = 1, 2
\end{aligned} \qquad [3.43]$$

where $g_{1\mathrm{I}}$, $g_{1\mathrm{T}}$, $g^i_{1\mathrm{A}}$ and $g^i_{1\mathrm{L}}$ $(i = 1, 2)$ are functions related to the interlimb coordination (see section 3.4.1.3) and $g^i_{2\mathrm{A}}$ and $g^i_{2\mathrm{L}}$ $(i = 1, 2)$ are functions related to phase resetting (see section 3.4.1.4).

3.4.1.2. *Pattern formation model*

In the PF model, we use the simple leg kinematics consisting of the swing and stance phases in reference to the length and orientation of the limb axis in the pitch plane (Figure 3.10). For the swing phase, the ankle pitch joint follows the simple closed curve, which includes an anterior extreme position (AEP) and a posterior extreme position (PEP). It starts from the PEP and continues until the foot touches the ground. During the stance phase, it traces out a straight line from the landing position (LP) to the PEP. In both the swing and stance phases, the angular movement of the ankle pitch joint is designed so that the foot is parallel to the line that connects points AEP and PEP.

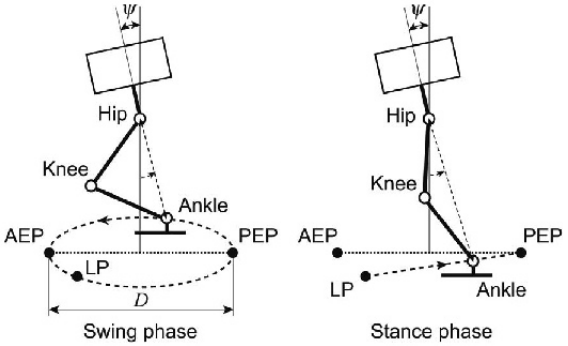

Figure 3.10. *Desired leg kinematics composed of the swing and the stance phases. When the foot lands on the ground, the trajectory changes from the swing to the stance phase. When the foot reaches the posterior extreme position (PEP), the trajectory moves into the swing phase*

We denote D as the distance between the AEP and PEP. We denote the swing and stance phase durations by T_{sw} and T_{st}, respectively, for the case that the foot touches the ground at the AEP (LP = AEP). The nominal duty factor β, which is the ratio between the stance phase and the gait cycle, the basic frequency ω, the stride length S, and the locomotion speed v are then given by:

$$\beta = \frac{T_{\mathrm{st}}}{T_{\mathrm{sw}} + T_{\mathrm{st}}}$$

$$\omega = \frac{2\pi}{T_{\mathrm{sw}} + T_{\mathrm{st}}}$$

$$S = \frac{T_{\text{sw}} + T_{\text{st}}}{T_{\text{st}}} D$$
$$v = \frac{D}{T_{\text{st}}} \qquad [3.44]$$

The trunk is at the angle of ψ to the line perpendicular to the line connecting the AEP and the PEP. From the inverse kinematics, the two trajectories for the swing and stance phases provide the desired angles of the hip, knee and ankle pitch joints of the leg i by the function of the phase ϕ_{L}^i of the leg i oscillator, where we use $\phi_{\text{L}}^i = 0$ at the PEP and $\phi_{\text{L}}^i = \phi_{\text{AEP}}$ $(= 2\pi(1-\beta))$ at the AEP.

To increase the stability of bipedal locomotion in three-dimensional space, we also use the hip and ankle roll joints. We design the desired angles by $R\cos(\phi_{\text{T}} + \varphi)$ using the phase ϕ_{T} of the trunk oscillator, where R is the amplitude of the roll motion and φ determines the phase relationship between the leg movements in the pitch and roll planes.

In our study, we deal with both bipedal and quadrupedal locomotion of a biped robot. For quadrupedal locomotion, the arm motions are also designed from the inverse kinematics using the shoulder and elbow pitch joints in a similar manner to the pitch joints of the legs.

3.4.1.3. *Interlimb coordination*

For the interlimb coordination, we use the desired phase relations by $\phi_{\text{A}}^1 - \phi_{\text{A}}^2 = \pi$, $\phi_{\text{L}}^1 - \phi_{\text{L}}^2 = \pi$ and $\phi_{\text{A}}^1 - \phi_{\text{L}}^2 = 0$ $(\phi_{\text{A}}^2 - \phi_{\text{L}}^1 = 0)$ so that both legs and arms generally move in antiphase, and one arm and the contralateral leg move in phase. The functions $g_{1\text{I}}$, $g_{1\text{T}}$, $g_{1\text{A}}^i$ and $g_{1\text{L}}^i$ in [3.43] are given as follows by using the phase differences between the oscillators based on the inter oscillator:

$$\begin{aligned} g_{1\text{I}} &= -\sum_{i=1}^{2} K_{\text{A}} \sin(\phi_{\text{I}} - \phi_{\text{A}}^i - (-1)^i \pi/2) \\ &\quad -\sum_{i=1}^{2} K_{\text{L}} \sin(\phi_{\text{I}} - \phi_{\text{L}}^i + (-1)^i \pi/2) \\ g_{1\text{T}} &= -K_{\text{T}} \sin(\phi_{\text{T}} - \phi_{\text{I}}) \\ g_{1\text{A}}^i &= -K_{\text{A}} \sin(\phi_{\text{A}}^i - \phi_{\text{I}} + (-1)^i \pi/2) \quad i = 1, 2 \\ g_{1\text{L}}^i &= -K_{\text{L}} \sin(\phi_{\text{L}}^i - \phi_{\text{I}} - (-1)^i \pi/2) \quad i = 1, 2 \end{aligned} \qquad [3.45]$$

where K_{L}, K_{A} and K_{T} are gain constants.

3.4.1.4. *Phase resetting*

As the sensory modulation based on phase resetting, when the foot of the leg i (the hand of the arm i) lands on the ground, the phase ϕ_{L}^{i} of the leg i oscillator (the phase ϕ_{A}^{i} of the arm i oscillator) is reset to ϕ_{AEP} at the landing ($i = 1, 2$). Therefore, the functions $g_{2\mathrm{A}}^{i}$ and $g_{2\mathrm{L}}^{i}$ in [3.43] are expressed as:

$$\begin{aligned} g_{2\mathrm{A}}^{i} &= (\phi_{\mathrm{AEP}} - \phi_{\mathrm{A}}^{i})\delta(t - t_{\mathrm{Aland}}^{i}) \quad i = 1, 2 \\ g_{2\mathrm{L}}^{i} &= (\phi_{\mathrm{AEP}} - \phi_{\mathrm{L}}^{i})\delta(t - t_{\mathrm{Lland}}^{i}) \quad i = 1, 2 \end{aligned} \qquad [3.46]$$

where t_{Lland}^{i} (t_{Aland}^{i}) is the time when the foot of the leg i (the hand of the arm i) lands on the ground ($i = 1, 2$). Note that the touch sensor signals not only modulate the locomotor rhythm and its phase but also switch the desired motion from the swing to the stance phase, as described in section 3.4.1.2.

3.4.2. *Experimental results*

To show the usefulness of our locomotion control system in the real world, we conducted various experiments using actual biped robots.

3.4.2.1. *Adaptive walking to environmental changes*

In this study, we used a biped robot, HOAP-1 (Fujitsu Automation Ltd.). We investigated if our locomotion control system produces adaptive walking to environmental changes, by discontinuously changing the slope angle of the floor [AOI 05]. Specifically, at the beginning the robot walked on a level surface, then on the slope and finally again on the flat surface. We employed two types of slope; upslope and downslope.

When we did not use phase resetting, the robot easily fell over. However, the robot with phase resetting achieved stable walking, as shown in Figures 3.11(a) and (b). Figures 3.11(c) and (d) show the profiles of the step cycle for upslope and downslope, respectively, revealing that the robot walks adaptively by changing the step cycle depending on the slope angle of the floor due to phase resetting. This adaptability is not a characteristic that we specifically designed, but it emerges through dynamic interaction between the robot's mechanical system, the oscillator control system and the environment.

3.4.2.2. *Adaptive turning walk*

Next, we dealt with turning walk using HOAP-1, where we established the turning walk by integrating straight and curved walk [AOI 07a]. Specifically, at the beginning the robot walks straight and then begins to circle to the left.

Its motion returns to straight walking and changes to curved walking to the right. Finally, it walks straight again. By regulating the number of steps for each walking pattern, the robot walks in a figure of eight.

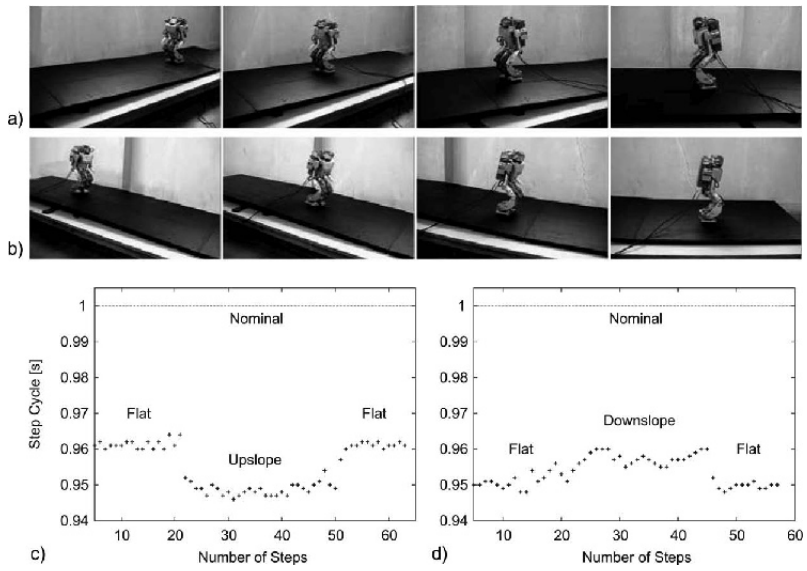

Figure 3.11. *Experimental result for discontinuously change of the floor's slope, where at the beginning the robot walks on the flat surface, then on the slope, and finally again on the flat surface. a) Snapshots for upslope and b) for downslope. c) Step cycle versus number of steps for upslope and d) for downslope*

Although the robot without phase resetting easily fell down, the robot with phase resetting achieved stable turning walk, as shown in Figure 3.12(a). Figure 3.12(b) shows the profile of the duty factors during the turning walk, revealing that the robot walks adaptively by changing the duty factors between straight and curved walk. Furthermore, the duty factors differ between the left and right legs for curved walk, similar to those observed in human curved walk [COU 03]. This adaptability also emerges through dynamic interaction between the robot mechanical system, the oscillator control system and the environment.

3.4.2.3. *Adaptive splitbelt treadmill walking*

To establish adaptive locomotion, interlimb coordination is an important factor. To investigate the mechanism controlling the interlimb coordination during walking, a splitbelt treadmill has been used [MOR 06, REI 05].

This treadmill is equipped with two parallel belts and the belt speeds can be controlled independently, which allows us to control the environmental situation to walk. We developed a biped robot and splitbelt treadmill for the robot and investigated the splitbelt treadmill walk of the robot [AOI 11a].

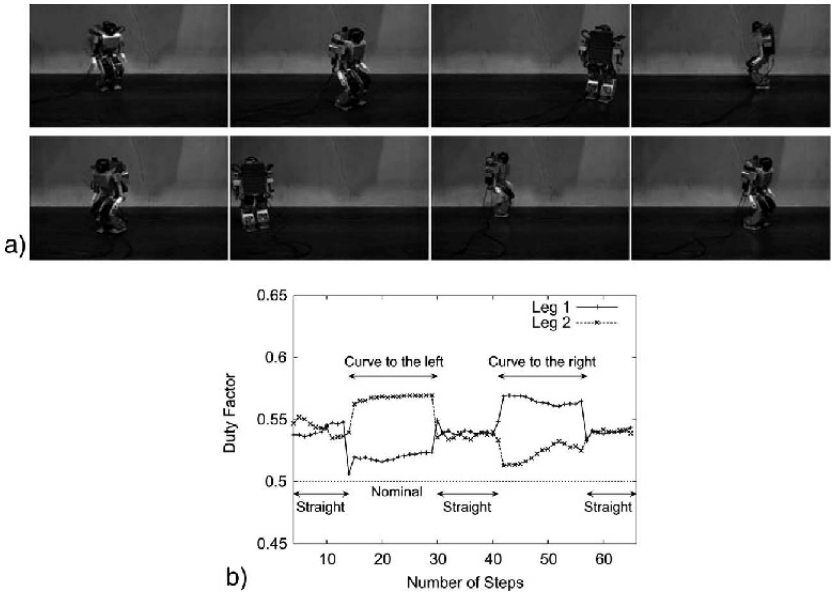

Figure 3.12. *Experimental result for turning walk, where the robot walks in a figure eight. a) Snapshots and b) duty factors versus number of steps*

When we did not use phase resetting, the robot easily fell down. However, the robot with phase resetting established stable walking despite a large discrepancy between the belt speeds. Instead, the relative phase between the leg movements shifted from antiphase and the duty factors of the legs varied depending on the speed discrepancy between the belts, similar to those observed in human splitbelt treadmill walking [MOR 06, REI 05].

3.4.2.4. *Adaptive gait transition from quadrupedal to bipedal locomotion*

Although many studies have investigated methods to achieve stable locomotor behaviors for various gaits, their transitions have not been thoroughly examined. In particular, the gait transition from quadrupedal to bipedal locomotion needs drastic changes in the robot posture and the reduction of the number of supporting limbs. Therefore, the stability greatly changes during the transition. To achieve such a gait transition, the following

two issues are crucial: (1) because a robot has many degrees of freedom, it is difficult to determine how to produce robot movements to connect one gait pattern to another, in other words, how to construct adequate constraint conditions in motion planning; (2) even if the robot establishes stable gait patterns, it may fall over during the gait transition and it is difficult to establish stable gait transition without falling over.

We applied our locomotion control system while incorporating the motion planning for the gait transition based on the physiological concept of kinematic synergy [ALE 98, FRE 06, FUN 10]. Similar to the above experiments, although the robot without phase resetting easily fell down, the robot with phase resetting achieved adaptive gait transition, as shown in Figure 3.13 [AOI 12].

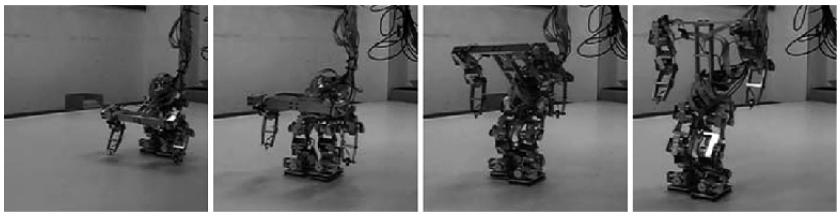

Figure 3.13. *Snapshots of the gait transition from quadrupedal to bipedal locomotion*

3.5. Conclusion

In this chapter, we designed a locomotion control system for a biped robot using nonlinear oscillators with phase resetting based on the physiological concept of CPG. We demonstrated the usefulness of this control system from the stability analysis using a simple biped robot model and from the experiments using actual biped robots. The stability analysis shows that the locomotion control system produces stable locomotor behavior and in addition shows that phase resetting improves stability for the gait parameters. The robot experiment shows that the locomotion control system using phase resetting produces adaptive walking of biped robots to environmental changes, such as discontinuous changes in slope angle and belt speeds of the splitbelt treadmill, and furthermore establishes adaptive turning walk and gait transition from quadrupedal to bipedal locomotion.

In locomotion of humans and animals, neuromechanical coordination is crucial. Although the phase resetting mechanism in biological systems remains unclear, we simply designed the sensory regulation model based

on phase resetting. Using phase oscillators allowed us to easily incorporate this to our locomotion control system. This modulates the locomotor rhythm depending on the foot contact information. In addition, this switches the desired kinematics from the swing phase to the stance phase. Because the swing and stance legs have different roles for locomotion dynamics, adequate timing to switch the desired kinematics is crucial. Despite this modulation being simple, it greatly contributes to generating various adaptive locomotor behaviors. In the future, we would like to employ a more sophisticated physical model and a biped robot to further clarify the stability mechanism and to construct a design principle to generate adaptive walking of legged robots.

3.6. Acknowledgments

This study is supported in part by a Grant-in-Aid for Scientific Research (B) No. 23360111 from the Ministry of Education, Culture, Sports, Science, and Technology of Japan, and by JST, CREST.

3.7. Bibliography

[ALE 98] ALEXANDROV A., FROLOV A., MASSION J., "Axial synergies during human upper trunk bending", *Experimental Brain Research*, vol. 118, pp. 210–220, 1998.

[AOI 05] AOI S., TSUCHIYA K., "Locomotion control of a biped robot using nonlinear oscillators", *Autonomous Robots*, vol. 19, no. 3, pp. 219–232, 2005.

[AOI 06a] AOI S., TSUCHIYA K., "Bifurcation and chaos of a simple walking model driven by a rhythmic signal", *International Journal of Non-Linear Mechanics*, vol. 41, no. 3, pp. 438–446, 2006.

[AOI 06b] AOI S., TSUCHIYA K., "Stability analysis of a simple walking model driven by an oscillator with a phase reset using sensory feedback", *IEEE Transactions on Robotics*, vol. 22, no. 2, pp. 391–397, 2006.

[AOI 07a] AOI S., TSUCHIYA K., "Adaptive behavior in turning of an oscillator-driven biped robot", *Autonomous Robots*, vol. 23, no. 1, pp. 37–57, 2007.

[AOI 07b] AOI S., TSUCHIYA K., "Self-stability of a simple walking model driven by a rhythmic signal", *Nonlinear Dynamics*, vol. 48, no. 1–2, pp. 1–16, 2007.

[AOI 10] AOI S., OGIHARA N., FUNATO T., *et al.*, "Evaluating functional roles of phase resetting in generation of adaptive human bipedal walking with a physiologically based model of the spinal pattern generator", *Biological Cybernetics*, vol. 102, no. 5, pp. 373–387, 2010.

[AOI 11a] AOI S., FUJIKI S., YAMASHITA T., *et al.*, "Generation of adaptive splitbelt treadmill walking by a biped robot using nonlinear oscillators with phase resetting", *Proceedings of IEEE/RSJ International Conference on Intelligent Robots and Systems*, pp. 2274–2279, 2011.

[AOI 11b] AOI S., TSUCHIYA K., "Generation of bipedal walking through interactions among the robot dynamics, the oscillator dynamics, and the environment: stability characteristics of a five-link planar biped robot", *Autonomous Robots*, vol. 30, no. 2, pp. 123–141, 2011.

[AOI 12] AOI S., EGI Y., SUGIMOTO R., *et al.*, "Functional roles of phase resetting in the gait transition of a biped robot from quadrupedal to bipedal locomotion", *IEEE Transactions on Robotics*, vol. 28, no. 6, pp. 1244–1259, 2012.

[BOS 01] BOSCO G., POPPELE R., "Proprioception from a spinocerebellar perspective", *Physiological Reviews*, vol. 81, pp. 539–568, 2001.

[BUR 01] BURKE R., DEGTYARENKO A., SIMON E., "Patterns of locomotor drive to motoneurons and last-order interneurons: clues to the structure of the CPG", *Journal of Neurophysiology*, vol. 86, pp. 447–462, 2001.

[COL 97] COLEMAN M., CHATTERJEE A., RUINA A., "Motions of a rimless spoked wheel: a simple three-dimensional system with impacts", *Dynamics and Stability of Systems*, vol. 12, no. 3, pp. 139–160, 1997.

[CON 87] CONWAY B., HULTBORN H., KIEHN O., "Proprioceptive input resets central locomotor rhythm in the spinal cat", *Experimental Brain Research*, vol. 68, pp. 643–656, 1987.

[COU 03] COURTINE G., SCHIEPPATI M., "Human walking along a curved path. II. Gait features and EMG patterns", *European Journal of Neuroscience*, vol. 18, no. 1, pp. 191–205, 2003.

[DUY 77] DUYSENS J., "Fluctuations in sensitivity to rhythm resetting effects during the cat's step cycle", *Brain Research*, vol. 133, no. 1, pp. 190–195, 1977.

[DUY 00] DUYSENS J., CLARAC F., CRUSE H., "Load-regulating mechanisms in gait and posture: comparative aspects", *Physiological Reviews*, vol. 80, pp. 83–133, 2000.

[FOR 73] FORSSBERG H., GRILLNER S., "The locomotion of the acute spinal cat injected with clonidine i.v.", *Brain Research*, vol. 50, pp. 184–186, 1973.

[FRE 06] FREITAS S., DUARTE M., LATASH M., "Two kinematic synergies in voluntary whole-body movements during standing", *Journal of Neurophysiology*, vol. 95, pp. 636–645, 2006.

[FUN 10] FUNATO T., AOI S., OSHIMA H., *et al.*, "Variant and invariant patterns embedded in human locomotion through whole body kinematic coordination", *Experimental Brain Research*, vol. 205, no. 4, pp. 497–511, 2010.

[GAR 98] GARCIA M., CHATTERJEE A., RUINA A., *et al.*, "The simplest walking model: stability, complexity, and scaling", *ASME Journal of Biomechanical Engineering*, vol. 120, no. 2, pp. 281–288, 1998.

[GOS 98] GOSWAMI A., THUILOT B., ESPIAU B., "A study of the passive gait of a compass-like biped robot: symmetry and chaos", *International Journal of Robotics Research*, vol. 17, no. 12, pp. 1282–1301, 1998.

[GRI 75] GRILLNER S., "Locomotion in vertebrates: central mechanisms and reflex interaction", *Physiological Reviews*, vol. 55, no. 2, pp. 247–304, 1975.

[GUE 95] GUERTIN P., ANGEL M., PERREAULT M.-C., *et al.*, "Ankle extensor group i afferents excite extensors throughout the hindlimb during fictive locomotion in the cat", *Journal of Physiology*, vol. 487, no. 1, pp. 197–209, 1995.

[IJS 07] IJSPEERT A., CRESPI A., RYCZKO D., *et al.*, "From swimming to walking with a salamander robot driven by a spinal cord model", *Science*, vol. 315, pp. 1416–1420, 2007.

[IJS 08] IJSPEERT A., "Central pattern generators for locomotion control in animals and robots: a review", *Neural Networks*, vol. 21, no. 4, pp. 642–653, 2008.

[KIM 07] KIMURA H., FUKUOKA Y., COHEN A., "Adaptive dynamic walking of a quadruped robot on natural ground based on biological concepts", *International Journal of Robotics Research*, vol. 26, no. 5, pp. 475–490, 2007.

[LAF 05] LAFRENIERE-ROULA M., MCCREA D., "Deletions of rhythmic motoneuron activity during fictive locomotion and scratch provide clues to the organization of the mammalian central pattern generator", *Journal of Neurophysiology*, vol. 94, pp. 1120–1132, 2005.

[LIU 08] LIU G., HABIB M., WATANABE K., *et al.*, "Central pattern generators based on Matsuoka oscillators for the locomotion of biped robots", *Artificial Life and Robotics*, vol. 12, no. 1, pp. 264–269, 2008.

[MOR 06] MORTON S., BASTIAN A., "Cerebellar contributions to locomotor adaptations during splitbelt treadmill walking", *Journal of Neuroscience*, vol. 26, no. 36, pp. 9107–9116, 2006.

[NAK 04] NAKANISHI J., MORIMOTO J., ENDO G., *et al.*, "Learning from demonstration and adaptation of biped locomotion", *Robotics and Autonomous Systems*, vol. 47, no. 2-3, pp. 79–91, 2004.

[NAK 06] NAKANISHI M., NOMURA T., SATO S., "Stumbling with optimal phase reset during gait can prevent a humanoid from falling", *Biological Cybernetics*, vol. 95, pp. 503–515, 2006.

[NOM 09] NOMURA T., KAWA K., SUZUKI Y., *et al.*, "Dynamic stability and phase resetting during biped gait", *Chaos*, vol. 19, pp. 026103-1–026103-12, 2009.

[ORL 99] ORLOVSKY G., DELIAGINA T., GRILLNER S., *Neuronal Control of Locomotion: From Mollusc to Man*, Oxford University Press, 1999.

[POP 02] POPPELE R., BOSCO G., RANKIN A., "Independent representations of limb axis length and orientation in spinocerebellar response components", *Journal of Neurophysiology*, vol. 87, pp. 409–422, 2002.

[POP 03] POPPELE R., BOSCO G., "Sophisticated spinal contributions to motor control", *Trends in Neurosciences*, vol. 26, pp. 269–276, 2003.

[REI 05] REISMAN D., BLOCK H., BASTIAN A., "Interlimb coordination during locomotion: what can be adapted and stored?", *Journal of Neurophysiology*, vol. 94, pp. 2403–2415, 2005.

[RYB 06a] RYBAK I., SHEVTSOVA N., LAFRENIERE-ROULA M., *et al.*, "Modelling spinal circuitry involved in locomotor pattern generation: insights from deletions during fictive locomotion", *Journal of Physiology*, vol. 577, no. 2, pp. 617–639, 2006.

[RYB 06b] RYBAK I., STECINA K., SHEVTSOVA N., *et al.*, "Modelling spinal circuitry involved in locomotor pattern generation: insights from the effects of afferent stimulation", *Journal of Physiology*, vol. 577, no. 2, pp. 641–658, 2006.

[SCH 98] SCHOMBURG E., PETERSEN N., BARAJON I., *et al.*, "Flexor reflex afferents reset the step cycle during fictive locomotion in the cat", *Experimental Brain Research*, vol. 122, no. 3, pp. 339–350, 1998.

[SHI 76] SHIK M., ORLOVSKY G., "Neurophysiology of locomotor automatism", *Physiological Reviews*, vol. 56, pp. 465–501, 1976.

[STE 10] STEINGRUBE S., TIMME M., WÖRGÖTTER F., *et al.*, "Self-organized adaptation of a simple neural circuit enables complex robot behaviour", *Nature Physics*, vol. 6, pp. 224–230, 2010.

[YAK 04] YAKOVENKO S., GRITSENKO V., PROCHAZKA A., "Contribution of stretch reflexes to locomotor control: a modeling study", *Biological Cybernetics*, vol. 90, pp. 146–155, 2004.

[YAM 03a] YAMASAKI T., NOMURA T., SATO S., "Phase reset and dynamic stability during human gait", *Biosystems*, vol. 71, pp. 221–232, 2003.

[YAM 03b] YAMASAKI T., NOMURA T., SATO S., "Possible functional roles of phase resetting during walking", *Biological Cybernetics*, vol. 88, pp. 468–496, 2003.